Article

Assessing the Protective Quality of Wax Coatings on Bronze Sculptures Using Hydrogel Patches in Impedance Measurements

Alice H. England, Kathryn N. Hosbein, Capri A. Price, Morgan K. Wylder, Kenna S. Miller and Tami Lasseter Clare *

Department of Chemistry, Portland State University, Portland, OR 97207, USA;
alice.england@gmail.com (A.H.E.); khosbein@pdx.edu (K.N.H.); capprice@pdx.edu (C.A.P.);
morgan.wylder@gmail.com (M.K.W.); kennasofiam@gmail.com (K.S.M.)
* Correspondence: claret@pdx.edu; Tel.: +1-503-725-2887

Abstract: In this work, we used chemically cross-linked acrylamide-based hydrogel patches that have been specifically developed for use as solid electrolytes in Electrochemical Impedance Spectroscopy to measure the impedance of two waxed bronze sculptures at the Seattle Art Museum's (SAM) Olympic Sculpture Park (OSP) and compare those results to laboratory test panels. We determined that the impedance response in the frequency range in which measurements may be taken (10 kHz to 1 MHz) is mostly capacitive and that a freshly applied wax coating should ideally be less than 1 nF·cm^{-2} for optimal protective performance.

Keywords: sculpture; wax; EIS; impedance; bronze; hydrogel; sensor; coating

1. Introduction

Protective coatings are applied to outdoor sculptures, structural and architectural metalworks to prevent corrosion and deterioration of the surface finish. Typically, collections care personnel rely upon visual cues such as rust staining, paint chalking or flaking to determine when re-applying a coating to a work is required. However, irreversible damage to the substrate has usually already occurred by the time such deterioration is visible. Developing methodologies to detect the early signs of coating failure is important to prevent aesthetic and ultimately structural damage to outdoor metalworks [1–3]. Ideally, such detection methodologies could be used in the field (without moving the object under study from its location), should be adaptable to multiple situations (e.g. textured, contoured, or inverted substrates), and should not require removing the protective coating to assess its protective qualities (non-destructive).

Chemically cross-linked hydrogels have recently gained attention in the artwork conservation field because of their adaptability and flexibility. In particular, hydrogels loaded with surfactant mixtures have been used for cleaning painted canvases via a mechanism of absorption into the surface layers, and, being chemically cross-linked, they leave no gel residue behind [4,5]. In electrochemical medical applications, hydrogels are commonly used in acquiring electrocardiograms (ECG), relying upon the potential transmitted through the skin caused by the depolarization of the heart cells' membranes [6]. In neither of those applications is direct access to the object under study (the painted layers or heart cells) required; the hydrogels are surface-mounted. Inspired by such applications, we have previously described the synthesis of hydrogels for use as surface-mounted solid electrolytes to monitor the protective quality of polymeric coatings on lab test panels using Electrochemical Impedance Spectroscopy (EIS) [7]. Because of its sensitivity to these small electrochemical changes, use of EIS for monitoring the barrier properties of protective coatings on metals is increasing [8–10].

However, the standard fluid cell technique is not well suited for field measurements because the use of rigid glass cells and direct electrical contact to the underlying metal is required. EIS has been previously applied to the study of metal art/archeological works in the context of developing new, improved coatings [3,11–14], and in one recent study in using commercial ECG gel patches as surface electrode(s) for in situ EIS [15]. While they are a cheap and convenient option, commercially available ECG electrodes (Ag/AgCl electrode surrounded by a conductive gel) are designed to have lower ion mobilities for use on skin and therefore must be pretreated with water or electrolyte for the measurement of high impedance coatings. Due to their high swelling capacity, exchange with the suitable electrolyte causes their structure to swell and weaken which makes them susceptible to tearing during the measurement. It also becomes difficult to accurately determine and reproduce the total electrolyte area in the gel's highly swollen state. In our previous work we demonstrated the synthesis of hydrogels specifically for use on cultural heritage material by optimizing their conductivity/electrode performance in a controlled swelling environment to create robust yet flexible electrode patches, which, we believe, is critical for the development of this field [16].

In this work, we utilize the optimized surface-mounted hydrogels in an EIS setup to monitor the protective quality of two waxed bronze sculptures at the Seattle Art Museum's Olympic Sculpture Park and compare those measurements with a variety of waxed and/or weathered and/or patinated bronze test panels. The OSP is a particularly aggressive corrosive environment, being located adjacent to the saltwaters of the Puget Sound and immersed in the urban atmosphere of downtown Seattle, WA, USA. The EIS data acquired from fieldwork at the OSP and the test panels were analyzed by creating equivalent electrical circuit (EEC) models for data fitting. Noise limited the frequency range of data acquired in the field, but we determined that the specific frequencies measured were accurate assessments of the capacitive quality of protective coatings. In general, coatings with poor barrier properties are able to accommodate and store excess charge in pores making them good capacitors, and therefore the most protective coatings will exhibit small capacitance values. Although there are degradation factors that instead decrease capacitance (i.e., the growth of large pores which may reduce the coating area under the electrodes), the increased coating dielectric from electrolyte uptake in pores during the impedance measurement will dominate and ultimately the capacitance will increase. In this study, we aimed to compare the capacitances (by measuring impedance and extracting the capacitance values) of waxed test panels with waxed sculptures and to observe any changes in the measured values after reapplication of a fresh wax coating on the sculptures. And since this is the first time that such information has been obtained on waxed sculptures in situ, we aimed to report these values to serve as benchmark values for wax coatings for comparison with future studies.

2. Materials and Methods

2.1. Outdoor Sculptures

EIS characterization of wax coatings on outdoor sculptures was conducted at the Olympic Sculpture Park (Seattle, WA, USA) in August 2013. *Persephone Unbound* (Beverly Pepper, 1999, 122″ × 31.5″ × 21″, 2009.14), a cast bronze sculpture (alloy unknown) with a light brown to gray patina and microcrystalline wax coating, was examined on the lower portion of the northeast face. The chair of *Untitled* (Roy McMakin, 2004–2007, 33″ × 22″ × 21.7″, 2006.32) was cast in silicon bronze (87300 Everdor) with a pigmented green patina. Microcrystalline wax coatings are applied annually by SAM conservation with the artist's permission. Sections on the chair's left arm and seat were tested both before and after the annual reapplication of the wax coating. *Persephone Unbound* was only measured prior to the wax reapplication. Photographs of the sculptures as well as detailed views of the specific areas measured are shown in Figure 1.
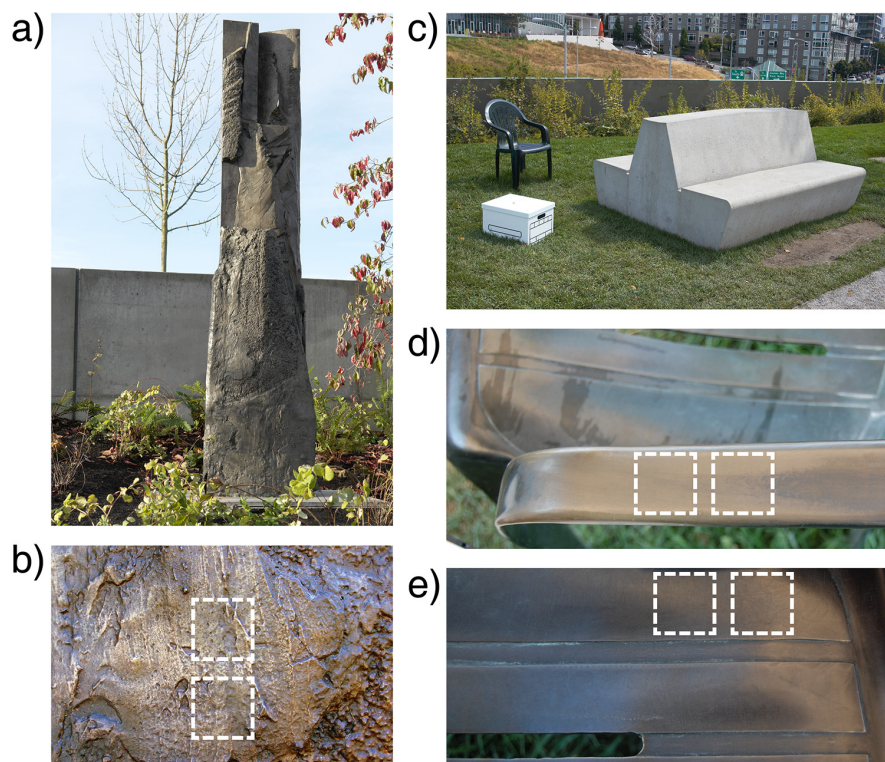
Figure 1. Photographs of the wax-coated bronze sculptures examined at the Olympic Sculpture Park: *Persephone Unbound* (**a**) and the chair in *Untitled* (**c**, top left corner). The specific areas (3 cm × 3 cm) tested are shown for Persephone Unbound (PPU) (**b**), C1 (**d**), and C2 (**e**), with the white squares marking the approximate areas tested in the Electrochemical Impedance Spectroscopy (EIS) experiments (i.e., the placement of the two hydrogel electrodes).

These sculpture measurements will be referred to as PPU (Persephone Unbound), C1 (chair arm), C2 (chair seat), C1b (chair arm after re-waxing), and C2b (chair seat after re-waxing), as summarized in Table 1. The thicknesses, reported in Table 1, measured with a PosiTector 6000 thickness gauge, represent the total thickness of the patina and wax coating together. PPU had a much higher thickness error resulting from the difficulty in obtaining consistent thickness readings on the highly textured sculpture surface.

Table 1. Summary of details for the Olympic Sculpture Park sculptures and test plates including the metal substrate, patina, coating material, aging method, and average coating thickness. The reported coating thickness is representative of the entire passive layer, which includes the protective coating (wax, B-44) and the patina if present.

	Sample	Metal	Patina	Coating	Aging Method	Thickness/μm
	PPU	Bronze	Yes	Microcrystalline wax	Outdoors	52.3 ± 27
	C1	Bronze	Yes	Microcrystalline wax	Outdoors	32.6 ± 2.9
Sculpture	C2	Bronze	Yes	Microcrystalline wax	Outdoors	42.6 ± 5.6
	C1b	Bronze	Yes	Microcrystalline wax	Outdoors	37.8 ± 6.4
	C2b	Bronze	Yes	Microcrystalline wax	Outdoors	39.9 ± 5.3
	W	Bronze	No	Renaissance wax	NA	11.2 ± 4.5
	B44	Bronze	No	B-44	NA	37.2 ± 3.5
Test	PA	Bronze	Yes	NA	QUV 500 hrs	3.8 ± 1.1
	WA	Bronze	No	Renaissance wax	QUV 1250 hrs	17.8 ± 2.6
	WPA	Bronze	Yes	Renaissance wax	QUV 1500 hrs	14.8 ± 5.2

2.2. Test Plates

For comparison with the sculpture park data, new wax and clear polymeric test coatings were prepared on phosphor bronze substrates (Alloy 521, 2.44 cm × 6 cm, 91%–92% Cu, 8% Sn, maximum 0.3% P, US Brass & Copper). The metal coupons were first cleaned by degreasing with p-xylene and acetone and then polished by sanding with 400 and 600 grit sandpaper to create a uniform surface. Fresh Renaissance wax (a microcrystalline wax blend of Cosmolloid 80 and BASF A waxes) was then directly applied using a cotton cloth in layers to the warmed bronze panel until the desired film thickness was achieved. A common polymer clear coating, Paraloid™ B-44 (binary copolymer resin of ethyl acrylate/methyl methacrylate, Dow, Inc., Midland, MI, USA), was applied to the second bronze substrate with a Fuji HVLP Super XPC™ spray gun. Final dry coating thicknesses are listed in Table 1 for the fresh wax (W) and the Paraloid™ B-44 (B44) coatings.

Aged test coatings were prepared on bronze coupons (2.54 cm × 7.62 cm, 90% Cu, 10% Sn, TB Hagstoz & Son, Inc.) that were cleaned and polished in the same manner as described above. For the patinated substrates the clean metal surface was treated with a 20% v/v solution of Antique Black (Birchwood Casey, Inc., Eden Prairie, MN, USA), rinsed with water and ethanol, and then dried with acetone and compressed air. Renaissance wax coatings were then applied as described above. Artificial weathering of the test panels was achieved in a Q-Lab QUV chamber with exposure to UV-B radiation and condensation cycles according to ASTM G154 Cycle 2. The patinated aged substrate (PA), which did not have an applied coating, was weathered for 500 QUV h; the waxed, aged plain (without a patina) substrate (WA) for 1250 QUV h; and the waxed, patinated aged substrate (WPA) for 1500 QUV h. The thicknesses summarized in Table 1 for these panels are for the coatings in their aged state.

2.3. Hydrogel Electrode Synthesis

All chemicals were obtained from Sigma-Aldrich and solutions were made using deionized H_2O. AMPS-co-PAA hydrogels were synthesized from the sodium salts of 2-acrylamido-2-methylpropanesulfonic acid (AMPS; 50 wt % solution) and poly (acrylic acid) (PAA; average MW 5100, 50 wt % solution). N,N'-methylenebis(acrylamide) (MBA; 1 wt % solution) was used as the cross-linker and the polymerization was carried out via the potassium persulfate and metabisulfite redox initiator system (1 wt % solutions) with glycerol added as a humectant. Details on the hydrogel component amounts and reaction conditions are documented in our previous publication [16]. After polymerization the 1 mm thick gel sheets were rinsed and equilibrated in 0.5 M dipotassium 1,4-piperazinediethanesulfonic acid (K_2PIPES) for 24 h to increase the hydrogel conductivity. K_2PIPES was determined to be the optimal electrolyte for this application due to its low risk of electrolyte-mediated substrate corrosion and high ratio of conductivity to swelling capacity that resulted in a suitably strong yet conductive hydrogel electrode material [16]. Equilibrated gel sheets were carefully removed from the K_2PIPES solution, dabbed gently with Kimwipes™ (Kimberly-Clark Professional, Roswell, GA, USA) to remove excess liquid on the surface, and then stored in an airtight container between transparency sheets. Hydrogels were cut into 3 cm × 3 cm squares as needed for use as solid electrolytes in the impedance measurements.

2.4. Electrochemical Impedance Spectroscopy

A simplified diagram of the hydrogel EIS cell created for in situ characterization of coated sculptures is shown in Figure 2a with a photograph in Figure 2b.

The cell consists of two hydrogel electrodes each backed with a strip of nickel foil (4 cm × 10 cm, 0.05 mm thick, annealed, 99+%, Alfa Aesar, Tewksbury, MA, USA) for connection to the working and counter electrode potentiostat leads. A translucent silicone rubber frame (1/32″ thick, McMaster-Carr) was placed around each hydrogel to maintain consistent electrode spacing (1.2 cm) and also to prevent damage to the hydrogels when the cell was pressed onto the sample surface. The complete

electrodes (foil, hydrogel, and silicone rubber spacers) were secured to a piece of soft polyurethane foam backed with stainless steel wire mesh that could be shaped to fit the contours of each sample surface. The entire cell was pressed onto the sample in the desired orientation by a pivoting plate on a flexible arm support, which allowed for the cell to be positioned securely without the use of any adhesive materials. Overall length of the foam backing piece was approximately 15 cm. Current flow is indicated by the arrow drawn between the hydrogel electrodes and the diagonal shading in the coating represents the areas probed during the measurement (i.e., the area underneath each hydrogel) in Figure 2a.
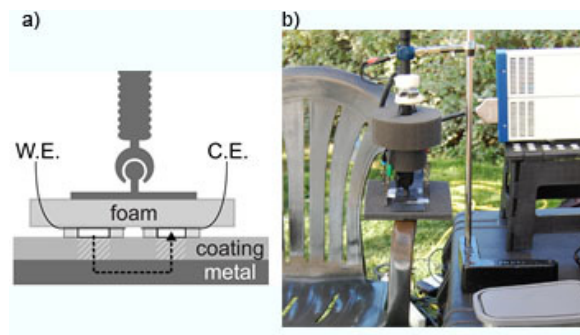
Figure 2. (**a**) Diagram of the hydrogel EIS cell used for both outdoor sculptures and test panels. Relative sizes of the components are exaggerated for illustrative purposes; (**b**) Photograph of the EIS cell being used during a measurement of C1.

Impedance spectra were recorded with a Gamry REF600 potentiostat from 1 MHz to 0.1 Hz with an applied AC potential of 20 mV$_{rms}$ versus the open circuit potential, where the reference electrode is connected to the counter electrode. The wax coatings on sculptures were measured outside in their natural conditions while the coatings on test panels were evaluated in the laboratory. Spectra were collected repeatedly for each system until the impedance stabilized (typically about 40 min), which indicated sufficient equilibration with the hydrogel and electrolyte. The final stable EIS spectra were normalized to the area component of the cell constant for a two-gel configuration

$$K_{\text{cell, area}} = 1/A_1 + 1/A_2 \tag{1}$$

where A_1 and A_2 are the areas of each gel electrode [16], and K_{cell} is therefore equal to $2/9$ cm^{-2} for this particular cell. Additionally, the impedance contribution of the hydrogel electrodes was determined by measuring the hydrogel cell alone on a completely conductive, non-corroding surface (silver foil). This background impedance (also area-normalized) originating from the hydrogel and the electrolyte double layer on the silver foil must be subtracted from each coating EIS spectrum. An example of this background correction is presented in further detail in the Section 3.1.

Normalized and background corrected EIS spectra were fit to equivalent electrical circuit models using the ZView software version 3.3c (Scribner Associates, Southern Pines, NC, USA). Model elements included resistors (*R*), Constant Phase Elements (*CPE*), and the infinite Warburg diffusion impedance (*W*), which have the following impedance relationships:

$$Z_R = R \tag{2}$$

$$Z_{CPE} = 1/Y_0 \, (i\omega)^{\alpha} \tag{3}$$

$$Z_W = \sigma/\sqrt{i\omega} \tag{4}$$

where R is the resistance in $\Omega \cdot$cm^2, Y_0 is the *CPE* parameter in units of S s$^{\alpha}$ cm^{-2} and α is a scaling factor between 0 and 1 ($\alpha = 1$ for an ideal capacitor), σ is the Warburg coefficient in units of $\Omega \cdot$cm$^2 \cdot$s$^{-1/2}$,

and ω is the angular frequency. The *CPE* is used instead of an ideal capacitor to better represent the non-ideality of the system and to improve the fits. Capacitance is calculated from the *CPE* parameters according to the following equation [17]:

$$C = Y_0 \left(\omega\right)^{(\alpha-1)} = Y_0 \left(2\pi f\right)^{(\alpha-1)} \tag{5}$$

where f is the frequency at which the imaginary impedance (Z'') reaches a maximum. In this work, however, there was no defined maximum Z'' and thus capacitance was calculated over select frequency ranges representing regions where the given capacitive element dominated, i.e., where the phase angle was closest to $-90°$. Further discussion of equivalent electrical circuit modeling for EIS of coatings and thin films can be found in the literature [18,19].

3. Results and Discussion

3.1. Hydrogel Cell Background Impedance

The hydrogel cell's characteristic impedance spectrum has been discussed in detail in our previous study [16], and is represented here as the gray spectra (which are mostly overlapping with the black spectra) in Figure 3.
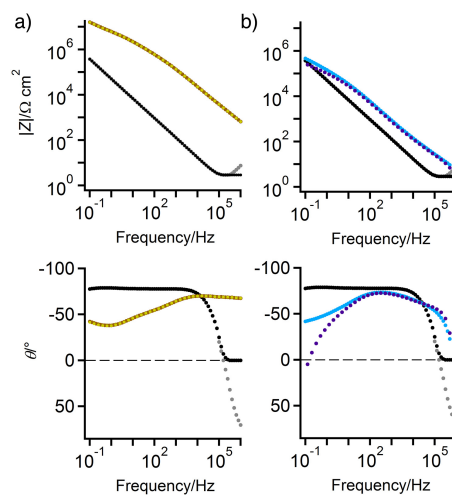
Figure 3. Impedance modulus and phase plots depicting the subtraction of the cell impedance from test panel spectra *W* (column a) and PA (column b). For all plots, both the cell impedance (gray) and the high frequency corrected cell impedance (black) are included for reference. In column (**a**), the *W* spectrum is shown both before (brown) and after (yellow) the subtraction of the corrected cell impedance. Similarly in column (**b**), the PA impedance is shown both before (blue) and after (purple) subtraction of the corrected cell spectrum.

Briefly, mutual inductance from the instrument cables is observed at the highest frequencies, followed by a resistive region that represents the bulk resistance of the hydrogel and electrolyte, and at frequencies less than 5 kHz the cell spectrum is dominated by the capacitance of the electrolyte double layer at the hydrogel/foil interface. Given that the high frequency inductance was an instrumental artifact, it was removed from the cell spectrum and the resistive region was extended to cover the higher frequencies as shown in the corrected cell spectra in Figure 3. For each system measured, the corrected cell impedance (Z_{cell}) was subtracted from the total impedance (Z_{tot}) for both the real (Z') and imaginary (Z'') components as shown in Equations (6) and (7).

$$Z'_{sub} = Z'_{tot} - Z'_{cell} \tag{6}$$

$$Z''_{sub} = Z''_{tot} - Z''_{cell}, \tag{7}$$

The background subtracted impedances (Z'_{sub}, Z''_{sub}) were then used to calculate the final impedance modulus, $|Z|$, and phase angle, θ, for each system using Equations (8) and (9).

$$|Z| = \sqrt{\left(Z'_{sub}\right)^2 + \left(Z''_{sub}\right)^2} \tag{8}$$

$$\theta = \arctan\left(Z''_{sub}/Z'_{sub}\right) \tag{9}$$

Background corrected EIS spectra for the test panels W and PA are presented in Figure 3a,b, respectively. When the system impedance is significantly higher than that of the cell, as was the case for *W*, then the cell subtraction is negligible and thus the spectra before and after the correction overlap almost completely (as can be seen in Figure 3a). For a lower impedance system, however, the subtraction of the cell EIS spectrum becomes necessary to separate the cell and system contributions. This is demonstrated in Figure 3b where the corrected PA spectrum is clearly different from the original, in particular at the low frequency end of the spectrum where the cell impedance reaches nearly the same value as the system. It becomes apparent that this background correction is necessary for accurate analysis of low Z systems, i.e., the PA system could erroneously be interpreted to have capacitive or diffusive properties at low frequencies while in reality the spectrum reflects the combination of the cell's capacitive behavior with the system's trend towards resistive behavior. Subtraction of the cell impedance was performed for all samples measured.

3.2. EIS of Wax-Coated Bronze Sculptures

The EIS spectra of *Persephone Unbound* (PPU) and the arm and seat areas of the chair (C1, C2) in *Untitled* using the hydrogel cell are presented in Figure 4a.
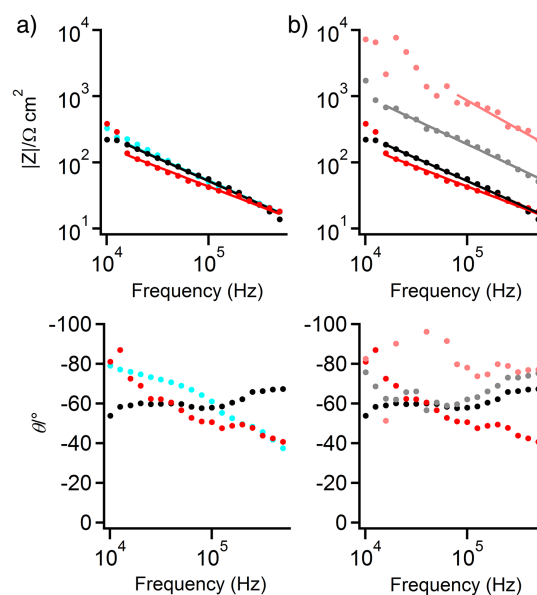

Figure 4. (**a**) Impedance modulus and phase plots of aged wax on the two different bronze sculptures, with the spectra displayed as solid circles for PPU (aqua), C1 (black), and C2 (red) and equivalent circuit fits included as solid lines in their same respective colors; (**b**) Bode plot comparison between the two areas measured on the chair before (C1, C2) and after (C1b, C2b) the annual wax reapplication. C1 and C2 are depicted in the same colors as in (a) along with C1b (gray) and C2b (pink) and their corresponding Constant Phase Elements (CPE) fit lines.

Only the high frequency data is shown, as the spectra exhibit a significant amount of noise below 10 kHz arising from outdoor electromagnetic noise coupled to the metal sculptures. Due to the large size of the sculptures it is not possible to shield the measurements with Faraday cages, and therefore

at this time the noise encountered at low frequencies cannot be avoided. Because of this, the EIS spectral analysis will focus on the high frequency end, which contains valuable information about the coating's electrochemical properties. All three of the aged wax coatings have similar impedance, and while the phase angle varies they all generally exhibit capacitive behavior. The spectra were modeled with a single CPE over a select frequency range where there was the least amount of noise, and the CPE parameters obtained from the fit are compiled in Table 2. The α value ranges from about 0.6–0.7, indicating that these waxes are not ideal capacitors ($\alpha = 1$). Using the CPE parameters, the capacitance was calculated using equation 6 at the high and low ends of the fit frequency range to obtain an approximate range of values for the capacitance of each system, which are listed in Table 2 and visualized in Figure 5a.

Table 2. CPE fit parameter values and errors for aged and fresh wax on bronze sculptures and the calculated capacitance range from equation 6 over the frequency range of the fits (316–15.9 kHz), except for C2b which was calculated over 1000–79.5 kHz due to the higher frequency onset of noise in the spectrum. The CPE parameter fitting errors are incorporated into the calculated capacitances, which are visualized in Figure 5a.

Sample	$Y_0/S\ s^{\alpha} \cdot cm^{-2}$	α	$C/nF \cdot cm^{-2}$
PPU	$1.84\ (\pm 0.492) \times 10^{-6}$	0.691 ($\pm$0.020)	10.7–40.6
C1	$1.97\ (\pm 0.234) \times 10^{-6}$	0.689 ($\pm$0.009)	18.7–60.5
C2	$8.32\ (\pm 1.59) \times 10^{-6}$	0.594 ($\pm$0.014)	18.6–92.7
C1b	$3.22\ (\pm 0.517) \times 10^{-7}$	0.728 ($\pm$0.012)	5.20–16.3
C2b	$1.19\ (\pm 0.276) \times 10^{-8}$	0.860 ($\pm$0.016)	1.21–2.94
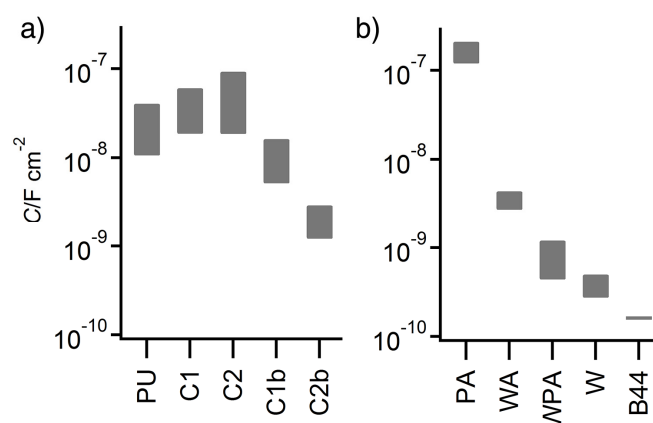
Figure 5. Comparison of calculated coating capacitance ranges for bronze sculptures (**a**) and test panels (**b**). The bars represent the capacitance range calculated using equation 6 at the high and low frequencies listed in Tables 2 and 3 for each sample, including the fitting errors from the CPE parameters.

PPU, C1 and C2 exhibited overlapping capacitance ranges, indicating that these aged wax coatings all have similar barrier properties, which is reasonable given that the waxes are exposed to similar weathering conditions in the outdoor park. It is important to note that the sample areas on each sculpture were of different orientation and surface finish. The hydrogel cell was able to record EIS spectra of wax on a vertically oriented, macroscopically rough surface (PPU, Figure 1b) and also on horizontal areas with smooth topography (C1 and C2, Figure 1d,e), which demonstrates the versatility of this methodology to accommodate the variety of sample conditions encountered on different sculptures.

The sample areas on the chair were also measured immediately after the annual reapplication of the wax coating to discern the differences in protective properties of aged and fresh wax on the same outdoor substrate. The freshly wax areas, C1b and C2b, are compared with the aged wax spectra

in Figure 4b. As expected, the fresh wax exhibited improved barrier properties, as evidenced by the increase in impedance when compared to the aged wax for each area. The fit parameters obtained from the CPE equivalent circuit model along with the calculated capacitance ranges are included in Table 2. When compared to their aged counterparts the fresh wax had lower capacitance in both cases, with C1b at about 1/3 of the aged value and with C2b decreasing by over an order of magnitude. The capacitors fitting the spectra became more ideal based on the increase in the α parameter after application of the fresh wax. The difference in the total amount of capacitive change between the two areas demonstrates the difficulty to produce an even wax layer on large-scale objects having surfaces of varying roughness and orientation. However, the fact that both areas exhibited higher impedance and reduced capacitance shows that the annual wax reapplication led to improved coating barrier properties and therefore better protection for the underlying sculpture. Although the frequency range for impedance detection was limited and the spectra were noisier than those typically recorded in the laboratory, this novel hydrogel EIS cell has allowed for meaningful characterization of wax coating performance on outdoor metal sculptures, specifically with regards to the high frequency capacitance.

3.3. EIS of Test Panels

A series of test panels were then measured with the hydrogel EIS cell in order to establish a better understanding of the absolute impedance values for new and aged wax coatings. EIS spectra for the three wax test panels (W, WA, WPA) are presented along with an uncoated specimen (PA) and a high-performance polymer coating (B44) in Figure 6a.
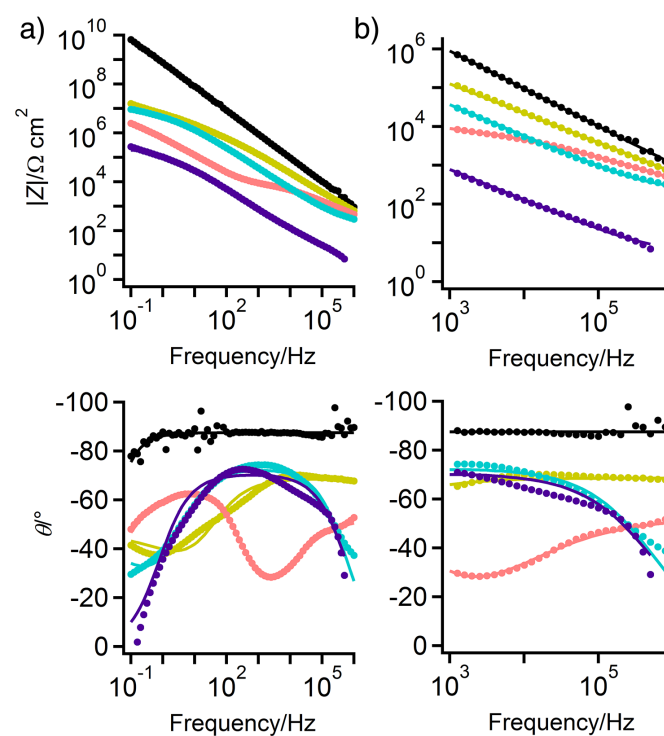
Figure 6. Impedance modulus and phase angle plots for test panels over the full frequency range (column a) and then expanded to show only the higher frequency impedance (column b). Spectra are shown as solid circles for PA (purple), WA (aqua), WPA (pink), W (chartreuse), and B44 (black), with the equivalent circuit fits included as solid lines in their same respective colors.

B44 exhibits the highest impedance overall, followed by the fresh wax (*W*), and then the plain (WA) and patinated (WPA) aged wax panels. PA recorded the lowest impedance at all frequencies, as expected due to the absence of a protective coating over the patina. The spectra were fit to equivalent

circuit models over the entire frequency range, however only the high frequency CPE can be used for comparison with the waxed sculpture EIS spectra due to the increased noise observed at lower frequencies in the measurements taken at the OSP. The complete circuit models and fitting parameters are included in the appendix for reference (Figure A1, Table A1), but the lower frequency elements will not be discussed in further detail here as only the higher frequency elements are relevant for comparison with the in situ measurements on the sculptures. An in-depth analysis of the full spectrum EIS response during weathering can be found in our recent study of waxed test panels using fluid cells [20]. It should be noted that the aged test panels, especially PA and WA, have larger errors in the model fits which is likely due to the complexity of the coating system. A coating with non-uniform degradation may exhibit areas with slightly different barrier properties which then results in the presence of multiple circuit elements with similar values that cannot be resolved in the model system. For the scope of this work, however, only the capacitive behavior at higher frequencies is of interest given that simpler analysis is the objective for impedance characterization of the coated sculptures.

The high frequency region of interest is shown in Figure 6b with the corresponding *CPE* fit parameters and calculated capacitances tabulated in Table 3. The capacitances observed range from 0.1 nF·cm^{-2} for B44 (most protective) up to 100 nF·cm^{-2} for PA (least protective). The waxes were more capacitive than B44, with the fresh wax at slightly lower values than the aged waxes. The protective qualities of these coatings can therefore be ranked as B44 > W > WPA > WA > PA, which is expected given that B44 films are amorphous polymers, lacking the crystalline grain boundaries of microcrystalline waxes and that aged waxes have reduced barrier properties compared to fresh wax [20].

Table 3. High frequency *CPE* fit parameters and errors for the test panels and the associated capacitances calculated from equation 6 over a frequency range where the *CPE* dominated the circuit for each panel. The *CPE* parameter fitting errors are incorporated into the calculated capacitances, which are visualized in Figure 5b.

Sample	Y_0/S s$^{\alpha}$·cm^{-2}	α	C/nF·cm^{-2}
PA	$1.33(\pm 0.043) \times 10^{-6}$	$0.785(\pm 0.0037)$	120–210 [a]
WA	$2.32(\pm 0.039) \times 10^{-8}$	$0.809(\pm 0.0018)$	2.74–4.41 [a]
WPA	$2.29(\pm 0.056) \times 10^{-7}$	$0.583(\pm 0.0017)$	0.438–1.20 [b]
W	$9.95(\pm 0.250) \times 10^{-9}$	$0.762(\pm 0.0022)$	0.274–0.498 [b]
B44	$2.27(\pm 0.028) \times 10^{-10}$	$0.972(\pm 0.0013)$	0.155–0.169 [c]

[a] Calculated at f = 10–1 kHz; [b] Calculated at f = 500–50 kHz; [c] Calculated at f = 100–10 kHz.

The high frequency capacitances calculated for the test panels are compared side-by-side with those of the waxed sculptures in Figure 5. The aged wax sculptures (PPU, C1, C2) have capacitances from about 10–100 nF·cm^{-2}, which is less than the uncoated test panel but not nearly as small as for the aged wax test panels. Upon reapplication of the wax (C1b, C2b) the capacitances decreased into the range of WA and WPA but did not reach that of the fresh wax test panel (<1 nF·cm^{-2}). This is likely due to the inherent challenges in achieving a uniform wax coating on a large-scale object where the existing wax is first removed (typically) and then the new coat is applied onsite in non-laboratory conditions. Although it may not be possible to match the low capacitance of a laboratory-applied wax test coating, its value can be used as a benchmark for conservators to aim for in their maintenance and care plans for wax-coated sculptures. For example, the hydrogel EIS cell would allow conservators to determine the optimal reapplication conditions (i.e., wax thickness, heat) by monitoring the high frequency capacitance and then refining the reapplication process until a minimum capacitance is reached. Changes in the capacitance over time would also provide critical information for conservators regarding the ideal time period between re-waxing for a given sculpture as variations in its outdoor microclimate likely influences the longevity of its protective coating.

4. Conclusions

We show that the protective quality of waxed sculptures and panels can be assessed using EIS with our hydrogel patches acting as the solid electrolyte. In the experimental setup described here, direct electrical contact to the substrate is not made, which is an enabling advantage of this technique. The measurable frequency range at OSP was nearly two orders of magnitude, where noise dominated at lower frequencies and instrumentation limited the higher frequency range. While the operable frequency range was short, we were, nonetheless, able to extract meaningful data from that range. Having a more limited measurement frequency range may serve to reduce instrumentation costs and simplify analysis, making the technique more widely accessible. The EIS signal obtained from the useful frequency range provides information on the capacitance of the coating, where smaller capacitances correspond to better protection against corrosion. In general, the capacitances of waxed coatings are larger than those of polymeric coatings, such as Paraloid™ B-44. After weathering outdoors for one year, the capacitance of the waxed chair of *Untitled*, was slightly smaller than an aged patinated non-coated test panel, suggesting that much of the wax's protective quality had been lost after that exposure period. After reapplication of the wax coating on the chair of *Untitled* (by SAM conservation staff), the capacitance of the coating decreased, but was approximately equivalent to waxed test panels that had been aged for over 1000 h in a QUV-B chamber. We suggest that capacitances of a freshly applied wax coating should ideally be less than 1 nF·cm^{-2} for acceptable protective performance. These results show that EIS measurements using the setup described here give insight into the protective quality of coatings as they exist on artwork. We have shown that EIS may be a useful tool to monitor the efficacy of coating treatments by comparing spectral changes before and after re-waxing and have provided a methodology to assess the protective lifetime of waxed coatings in situ and in real time.

Author Contributions: Tami Lasseter Clare and Alice H. England conceived and designed the experiments; Alice H. England, Kathryn N. Hosbein, Capri A. Price, and Morgan K. Wylder performed the OSP experiments; Alice H. England, Kathryn N. Hosbein, and Kenna S. Miller performed the test plate experiments; Alice H. England analyzed the data and, together with Tami Lasseter Clare, wrote the paper.

Conflicts of Interest: The authors declare no conflict of interest.

Appendix A
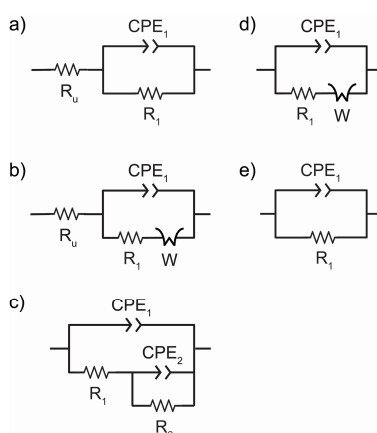
Figure A1. Equivalent circuit models used to for EIS spectra for PA (**a**), WA (**b**), WPA (**c**), W (**d**), and B44 (**e**). All resistor, constant phase element, and infinite Warburg parameters obtained from fitting are compiled in Table A1.

Table A1. Complete fitting parameters and error values from the equivalent circuit models in Figure A1 for each test panel. The circuit elements included are R_u (uncompensated resistance), CPE_1, R_1, CPE_2, and R_2. For WA and W the Warburg element parameters are listed under CPE_2 where α_2 is fixed at 0.5 and $Y_{0,2} = 1/\sigma$.

Sample	$R_u/\Omega\cdot cm^2$	$Y_{0,1}/S\ s^\alpha\cdot cm^{-2}$	α_1	$R_1/\Omega\cdot cm^2$
PA	5.46 ($\pm$0.474)	1.33 ($\pm$0.043) $\times 10^{-6}$	0.785 ($\pm$0.0037)	2.15 ($\pm$0.076) $\times 10^5$
WA	220 ($\pm$5.37)	2.32 ($\pm$0.094) $\times 10^{-8}$	0.809 ($\pm$0.0018)	4.62 ($\pm$0.142) $\times 10^6$
WPA	–	2.29 ($\pm$0.056) $\times 10^{-7}$	0.583 ($\pm$0.0017)	1.03 ($\pm$0.011) $\times 10^4$
W	–	9.95 ($\pm$0.250) $\times 10^{-9}$	0.762 ($\pm$0.0022)	2.36 ($\pm$0.096) $\times 10^6$
B44	–	2.27 ($\pm$0.028) $\times 10^{-10}$	0.972 ($\pm$0.0013)	3.22 ($\pm$0.512) $\times 10^{10}$

Sample	$Y_{0,2}/S\ s^\alpha\cdot cm^{-2}$	α_2	$R_2/\Omega\cdot cm^2$
PA	–	–	–
WA	1.73 ($\pm$0.061) $\times 10^{-7}$	0.5	–
WPA	2.22 ($\pm$0.042) $\times 10^{-7}$	0.786 ($\pm$0.0026)	8.97 ($\pm$0.242) $\times 10^6$
W	7.34 ($\pm$0.131) $\times 10^{-8}$	0.5	–
B44	–	–	–

References

1. Otieno-Alego, V.; Health, G.; Hallam, D.; Creagh, D. Electrochemical evaluation of the anti-corrosion performance of waxy coatings for outdoor bronze conservation. In Proceedings of the International Conference on Metals Conservation, Draguignan, France, 27–29 May 1998; pp. 309–314.
2. Cano, E.; Bastidas, D.M.; Argyropoulos, V.; Fajardo, S.; Siatou, A.; Bastidas, J.M.; Degrigny, C. Electrochemical characterization of organic coatings for protection of historic steel artefacts. *J. Solid State Electrochem.* **2010**, *14*, 453–463. [CrossRef]
3. Cano, E.; Lafuente, D.; Bastidas, J.M. Use of EIS for the evaluation of the protective properties of coatings for metallic cultural heritage: A review. *J. Solid State Electrochem.* **2010**, *14*, 381–391. [CrossRef]
4. Domingues, J.; Bonelli, N.; Giorgi, R.; Baglioni, P. Chemical semi-IPN hydrogels for the removal of adhesives from canvas paintings. *Appl. Phys. A Mater. Sci. Process.* **2014**, *114*, 705–710. [CrossRef]
5. Pizzorusso, G.; Fratini, E.; Eiblmeier, J.; Giorgi, R.; Chelazzi, D.; Chevalier, A.; Baglioni, P. Physicochemical Characterization of Acrylamide/Bisacrylamide Hydrogels and Their Application for the Conservation of Easel Paintings. *Langmuir* **2012**, *28*, 3952–3961. [CrossRef] [PubMed]
6. Alba, N.A.; Sclabassi, R.J.; Sun, M.G.; Cui, X.T. Novel Hydrogel-Based Preparation-Free EEG Electrode. *IEEE Trans. Neural Syst. Rehabil. Eng.* **2010**, *18*, 415–423. [CrossRef] [PubMed]
7. England, A.E.; Clare, T.L. Synthesis and Characterization of Flexible Hydrogel Electrodes for Electrochemical Impedance Measurements of Protective Coatings on Metal Sculptures. *Electroanalysis* **2014**, *26*, 1059–1067. [CrossRef]
8. Mansfeld, F.; Kendig, M.W. *Electrochemical Impedance Tests for Protective Coatings*; Laboratory Corrosion Tests and Standards; ASTM International: Philadelphia, PA, USA, 1985; pp. 122–142.
9. Amirudin, A.; Thierry, D. Application of electrochemical impedance spectroscopy to study the degradation of polymer-coated metals. *Prog. Org. Coat.* **1995**, *26*, 1–28. [CrossRef]
10. Van Westing, E.P.M.; Ferrari, G.M.; de Wit, J.H.W. The determination of coating performance with impedance measurements-I. Coating polymer properties. *Corros. Sci.* **1993**, *34*, 1511–1530. [CrossRef]
11. Swartz, N.A.; Clare, T.L. Understanding the differences in film formation mechanisms of two comparable solvent based and water-borne coatings on bronze substrates by electrochemical impedance spectroscopy. *Electrochim. Acta* **2012**, *62*, 199–206. [CrossRef]
12. Price, C.; Hallam, D.; Heath, G.; Creagh, D.; Ashton, J. An electrochemical study of waxes for bronze sculpture. In Proceedings of the International Conference on Metals Conservation, Semur en Auxois, France, 25 September 1997; pp. 233–241.
13. Letardi, P.; Beccaria, A.; Marabelli, M.; Ercolo, G.D. Application of electrochemical impedance mesurements as a tool for the characterization of the conservation and protection state of bronze works of art. In Proceedings of the International Conference on Metals Conservation, Draguignan, France, 27–29 May 1998; pp. 303–308.

14. Clare, T.L. Evaluation of fluorinated protective coatings for outdoor metals. In Proceedings of the International Conference on Metals Conservation, Amsterdam, The Netherlands, 23–26 October 2007; pp. 83–87.

15. Corbellini, S.; Parvis, M.; Grassini, S. Noninvasive Solution for Electrochemical Impedance Spectroscopy on Metallic Works of Art. *IEEE Trans. Instrum. Meas.* **2012**, *61*, 1193–1200. [CrossRef]

16. England, A.H.; Clare, T.L. Synthesis and characterization of flexible hydrogel electrodes for electrochemical impedance measurements of protective coatings on metal sculptures. *Electroanal* **2014**, *26*, 1059–1067. [CrossRef]

17. Hsu, C.H.; Mansfeld, F. Technical note: Concerning the conversion of the constant phase element parameter Y-0 into a capacitance. *Corrosion* **2001**, *57*, 747–748. [CrossRef]

18. Walter, G.W. A review of impedance plot methods used for corrosion performance analysis of painted metals. *Corros. Sci.* **1986**, *26*, 681–703. [CrossRef]

19. Freger, V.; Bason, S. Characterization of ion transport in thin films using electrochemical impedance spectroscopy. I. Principles and theory. *J. Membr. Sci.* **2007**, *302*, 1–9. [CrossRef]

20. Swartz, N.A.; Clare, T.L. On the protective nature of wax coatings for culturally significant outdoor metalworks. *J. Am. Inst. Conserv.* **2015**, *54*, 181–201. [CrossRef]